Egyptian Journal of Aquatic Biology & Fisheries
Zoology Department, Faculty of Science,
Ain Shams University, Cairo, Egypt.
ISSN 1110 – 6131
Vol. 28(1): 1041 – 1062 (2024)
www.ejabf.journals.ekb.eg

Seasonal Heat and Buoyancy Fluxes in the Red Sea

Fahmy Eid*, Radwa Dahy, Magdy Farag, Mohamed Shaltout
Oceanography Department, Faculty of Science, Alexandria University, Egypt
***Corresponding Author:** fahmyeid2@yahoo.com

ARTICLE INFO

Article History:
Received: May 31, 2023
Accepted: Nov. 30, 2023
Online: Jan. 30, 2024

Keywords:
Red Sea,
Evaporation,
Heat flux,
Buoyancy flux

ABSTRACT

The variations of thermal and haline buoyancy fluxes were investigated in the Red Sea. Analyses were performed to determine whether or not thermal buoyancy flux resulting from the net heat flux or haline buoyancy flux arising from freshwater flux dominates in the net buoyancy flux of the Red Sea. The effect of the two types of buoyancy flux was examined using Hybrid Coordinate Ocean Model (HYCOM) water temperature and salinity data at a resolution of ≈3.2km during the years 2019 and 2020. The monthly mean atmospheric data were taken from the European Center for Medium-range Weather Forecast (ECMWF) Re-analyses (ERA5-data). The evaporation rate in the Red Sea gradually decreased from north to south. The annual average evaporation rate for the Red Sea as a whole was 0.45cm/ day (1.64m/ year). The monthly average values of net heat flux for the Red Sea as a whole showed a heat loss from the Red Sea during winter months and heat gain during the rest of the year. The annual mean of net heat flux for the Red Sea as a whole showed a heat gain with an average value of about 61.6Wm^{-2}. The net surface buoyancy flux destabilized the water column in January, February, November and December, which is an indication of the generation of strong convective mixing during these months. It stabilized the water column in the rest of the year, which means a stratification of the water column and shallow mixed layer depths. The buoyancy flux results also revealed that the thermal buoyancy flux dominated the haline buoyancy flux in all months over the Red Sea as a whole except for March 2019 in the Center Red Sea (CRS-region), October 2019 in the North Red Sea (NRS-region), January 2020 in the South Red Sea (SRS) and Entrance Red Sea (ERS-regions), and February 2020 in the CRS-region. During these exceptions, the region-averaged absolute ratio of the former to the latter was < 1 in the Red Sea. On the contrary, large buoyancy ratio values of ≫1 in other months explained that the buoyancy was much more sensitive to variations in heating.

INTRODUCTION

The atmosphere and the ocean form a coupled system, exchanging at the air-sea interface gases, water, particles, momentum and energy. These exchanges affect the biology, chemistry, and physics of the ocean, moreover it influences its biogeochemical processes, weather, and climate. Furthermore, the air-sea interaction is one of the important processes that affect both atmospheric and oceanic variability. The atmosphere may affect sea surface temperature (*SST)* and upper-temperature stratification through

changing ocean surface heat fluxes. The ocean may affect the atmospheric convection and associated thermodynamic distributions by changing the boundary layer stability.

Karstensen and Lorbacher (2011) emphasized the importance of buoyancy flux in analyzing the mechanisms of ocean-atmosphere interactions. The buoyancy flux plays an important role in water mass transformation, mixing, stratification of water levels **(Zhang & Talley, 1998; Karstensen & Lorbacher, 2011)**, gas transfer in ocean **(MacIntyre *et al*., 2010)**, vertical nutrient transport **(Geng *et al*., 2019)**, and then in the upwelling. One of the challenges involving the buoyancy flux study for a particular region is relative to the determination of the quantity that allows capturing the relative contribution of the two components (thermal and haline) of the buoyancy flux in one single quantity **(Gill, 1982; Cronin & Sprintall, 2001; Anitha *et al*., 2008; Karstensen & Lorbacher, 2011)**.

Buoyancy flux through the surface helps determine the stability of the upper ocean. At the sea surface, surface warming (heat gain by the ocean) or precipitation tends to make the ocean surface more buoyant and contributes to stable conditions. Conversely, surface cooling or evaporation tends to make the ocean surface less buoyant and contributes to an increase in density of the surface water, consequently to a convectively unstable condition.

Surface momentum and buoyancy fluxes are generally the major drivers of mixing in the near-surface layer and the oceanic mixed layer development **(Cronin & Sprintall, 2008)**.

The main aim of this work was to study the contribution of heat flux and salinity flux to the total flux of surface buoyancy in the Red Sea.

MATERIALS AND METHODS

i- Study area

The Red Sea (RS) is an elongated semi-enclosed basin, which extends from 12.5°N to 30°N in the NW-SE direction with an average width of 280km. It has an average depth of 524m although maximum depths along the axial trench may exceed 3000m. A very shallow and narrow constriction, the Strait of Bab-al-Mandeb, connects the RS to the Gulf of Aden and through it to the Indian Ocean (Fig. 1). The RS connects to the Gulf of Aqaba in the northeast and the Gulf of Suez in the northwest (Fig. 1).

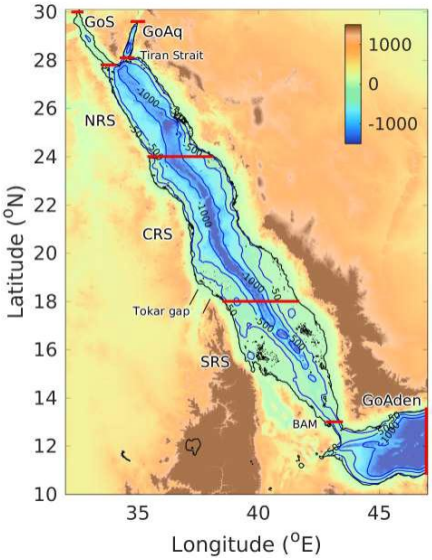

Fig. 1. The Red Sea bathymetry and regions

ii- Data used

a- Meteorological data

The monthly atmospheric data (sea surface temperature, air temperature, dew point temperature, cloud cover, atmospheric pressure at the surface, and zonal and meridional components of wind) for the computation of the surface net heat flux were taken from the European Center for Medium-Range Weather Forecasts (ECMWF) ERA5 with grid (0.25°x0.25°) for the two years of 2019 and 2020 **(Hersbach *et al*., 2020)**. website (https://cds.climate.copernicus.eu/cdsapp#!/ dataset/reanalysis-era5-single levels? tab= form).

b- Hydrographic data

The surface water temperature and salinity in the Red Sea throughout the two years period 2019- 2020 with grid size of 0.25°x0.25° were taken from Hybrid Coordinate Ocean Model (HYCOM) to examine buoyancy fluxes. The details of HYCOM equations are presented in **Bleck (2002)**, while the vertical coordinate evaluation for HYCOM is discussed in **Chassignet *et al*. (2003)**, and the vertical mixing algorithms are provided in **Halliwell (2004)**.

For ease of explanation, the Red Sea is divided into four regions: northern (24° N-28° N) (NRS), central (18° N-23° N)(CRS), southern (13° N-17° N) (SRS), and entrance (11° N-12° N) (ERS) regions (Fig. 1), and the seasons are defined as winter (Dec- Mar), spring (Apr- May), summer (Jun- Sep), and fall (Oct- Nov).

iii- Method of analysis

i. Surface heat flux

The net surface heat flux entering the ocean (Q_n) included solar radiation (Q_s), net longwave radiation (Q_b), latent heat flux resulting from evaporation (Q_e), and sensible heat flux arising from the air and water having different surface temperatures (Q_c):

$$Q_n = Q_s + Q_b + Q_e + Q_c \quad (1)$$

The short-wave radiation flux (Qs) and the net long-wave radiant flux (Q_b) were calculated by using the formulas of **Naoki *et al*. (1996)**. To calculate the vaporization latent heat flux, (Q_e) and the sensible heat, flux (Qc), the formula of **Naoki *et al*. (1996)**, **Simonsen and Haugan (1996)**, **Kara (2004)**, **Emery *et al*. (2005)** and **Mehrfar *et al*. (2007)** are used.

ii. Buoyancy flux

The buoyancy flux (BF), as defined by **Da Silva *et al*. (1994)**, is expressed as:

$$BF = -g \alpha Q_n / (\rho C_p) + g \beta (E - P) S_o \quad (2)$$

Where, BF has unit $m^2 s^{-3}$; Qn is the net surface heat flux (W/ m^2); g is the acceleration due to gravity; ρ is the density of water at the sea surface; c_P is the specific heat capacity of water; S_o, is the sea surface salinity (psu); rate of evaporation (E) and precipitation (P) have unit $m\ s^{-1}$ and α and β, the thermal expansion ($°C^{-1}$) and haline contraction (psu^{-1}) coefficients which are defined as follows:

$$\alpha = -\frac{1}{\rho}\frac{\partial \rho}{\partial T} \quad ; \quad \beta = \frac{1}{\rho}\frac{\partial \rho}{\partial S} \quad (3)$$

Values for ρ, C_p , α and β have been determined using equations presented in **Gill (1982)**.

When there is heat loss from the ocean ($Q_n < 0$) and net evaporation (E> P), positive values for BF occur, leading to an increase in the density of the near surface layer. Positive (negative) buoyancy flux indicates a buoyancy loss (gain). Thus, an increase in density of the ocean surface corresponds to buoyancy loss. Surface density increases (i.e., water column is destabilized) if BF> 0, and surface density decreases (i.e., water column is stabilized) if BF< 0.

The buoyancy flux BF consists of two terms: (1) thermal buoyancy flux (BT), and (2) haline buoyancy flux (BS). The thermal buoyancy flux is the buoyancy due to the net heat flux at the sea surface, and the haline buoyancy flux is the one due to the net freshwater flux at the sea surface. Thus, the total buoyancy is rewritten as follows:

$$BF = -g\alpha Q_n/(\rho c_p) \underline{\textit{(Thermal buoyancy flux)}} + g \beta (E-P) S_o \underline{\textit{(Haline buoyancy flux)}} \quad (4)$$

$$BF = BT + BS$$

A negative (i.e. downward) buoyancy flux, due to either surface warming or precipitation, tends to make the ocean surface more buoyant. Conversely, a positive buoyancy flux, due to either surface cooling or evaporation, tends to make the ocean surface less buoyant. Buoyancy loss from water column can lead to convective instability, with heavier water overlying lighter water. Turbulence, generated by the

ensuing convective overturning, can then cause deeper, generally cooler, water to be entrained and mixed into the surface mixed layer. Thus, entrainment mixing typically causes the SST to cool and the mixed layer to deepen.

The buoyancy flux, BF, determines the stability of the upper ocean, and it is possible to determine whether the thermal (BT) or haline (BS) component is the main contributor. The absolute value of the buoyancy ratio (|R|) of the thermal and haline buoyancy flux components is expressed by:

$$|R| = |(\alpha Q_n / c_p \rho \beta S_o (E-P))| \quad (5)$$

The ratio |R| indicates the relative impact of heating and salinity effects on upper ocean buoyancy. |R| ≈1 (i.e., the absolute value of the ratio which is on order of unity) explains that the buoyancy appears to be equally affected by heating and salinity effects. In other words, heat and freshwater fluxes are of the same magnitude. In a similar analogy, heat flux dominates freshwater flux when |R|> 1 (i.e., the buoyancy is due mostly to net heat flux at the sea surface), and freshwater flux dominates heat fluxes when |R|< 1 (i.e., the buoyancy is due mostly to net freshwater flux at the sea surface).

RESULTS

1. Heat budget terms (Seasonal evaporation and heat budget terms)

The seasonal variations of evaporation rate and heat budget terms over the study area during 2019 and 2020 are listed as average values for each season and all year at different regions of the study area and the study area as a whole (Tables 1- 3).

1.1. Seasonal evaporation rate

Tables (1- 3) show the average evaporation at different regions of the study area and over the Red Sea as a whole for each season during 2019 and 2020. The sea-air temperature differences (temperature gradient) play the main role in the differences in evaporation values at different regions of the study area.

During winter

The rate of evaporation decreased southward. It is higher in 2019 than in 2020 at NRS-region and CRS-region. The pattern is reversed at the SRS region and ERS-region. The evaporation rate over the Red Sea as a whole is higher during 2019 (0.57cm/ day) than 2020 (0.53cm/ day).

Table 1. Seasonal average of evaporation and heat budget terms at different regions of the Red Sea during winter and spring 2019- 2020

			2019						2020					
SEASON	REGION		E	QS	QB	QE	QC	QN	E	QS	QB	QE	QC	QN
			(CM/D)	W/m^2					(CM/D)	W/m^2				
WIN	N	AV	0.80	190.45	98.87	224.49	24.74	-157.64	0.67	194.26	95.54	187.59	19.78	-108.65
		STD	0.12	4.46	10.20	34.21	7.39	45.72	0.10	5.68	8.41	26.60	6.97	36.96
	C	AV	0.62	209.67	75.68	172.48	15.75	-54.24	0.58	212.89	77.14	163.07	14.14	-41.47
		STD	0.18	8.27	8.27	50.13	7.10	71.23	0.11	6.45	6.09	30.14	3.89	42.70
	S	AV	0.36	231.41	61.91	101.79	4.14	63.57	0.39	230.84	64.87	110.36	6.56	49.05
		STD	0.09	5.17	2.91	26.38	3.46	22.85	0.07	4.96	3.59	18.86	2.89	17.99
	E	AV	0.34	241.84	62.37	95.88	7.21	76.38	0.36	239.14	63.18	102.37	7.90	65.69
		STD	0.03	1.88	2.32	9.67	1.46	12.21	0.03	2.04	1.78	8.50	1.03	9.95
	RS	AV	0.57	213.84	76.20	158.54	13.87	-34.77	0.53	215.7	76.9	149.0	12.8	-23.1
		SD	0.22	18.09	15.86	61.84	9.84	100.87	0.15	15.9	13.2	40.8	6.7	71.7

			2019						2020					
SEASON	REGION		E(CM/D)	QS	QB	QE	QC	QN	E(CM/D)	QS	QB	QE	QC	QN
			(CM/D)	W/m^2					(CM/D)	W/m^2				
SPR	N	AV	0.37	292.84	68.15	103.73	-1.16	122.12	0.36	292.83	66.89	100.03	-1.15	127.06
		STD	0.06	0.82	8.44	17.68	3.97	24.83	0.06	0.52	7.29	16.73	3.55	22.73
	C	AV	0.30	294.24	58.56	83.95	2.58	149.15	0.33	293.25	58.30	92.88	2.15	139.92
		STD	0.04	0.20	4.37	11.94	2.04	15.83	0.05	0.32	4.05	13.06	2.18	15.93
	S	AV	0.32	292.14	50.66	88.35	-0.09	153.22	0.32	289.32	49.92	88.56	1.53	149.31
		STD	0.09	1.21	3.69	25.42	4.61	24.07	0.07	2.32	4.78	18.45	3.56	20.24
	E	AV	0.28	286.91	50.88	77.68	5.28	153.07	0.28	278.18	46.16	77.41	3.25	151.37
		STD	0.02	0.84	3.60	5.94	0.70	8.85	0.04	2.52	3.74	11.64	0.94	15.82
	RS	AV	0.32	292.74	57.97	89.47	1.12	144.19	0.33	290.9	57.0	92.2	1.3	140.4
		SD	0.07	2.06	8.57	19.71	3.91	23.88	0.06	4.3	8.6	16.6	3.2	20.7

Table 2. Seasonal average of evaporation and heat budget terms at different regions of the Red Sea during summer and autumn 2019- 2020

			2019						2020					
SEASON	REGION		E	QS	QB	QE	QC	QN	E(	QS	QB	QE	QC	QN
			(CM/D)	W/m^2					(CM/D)	W/m^2				
SUM	N	AV	0.44	293.49	52.16	122.84	-4.55	123.04	0.38	293.45	50.96	105.49	-5.93	142.94
		STD	0.08	0.28	8.84	23.67	4.47	30.82	0.08	0.26	8.51	23.19	4.66	28.82
	C	AV	0.40	290.72	43.26	111.60	-3.90	139.76	0.35	288.33	43.49	98.58	-2.94	149.20
		STD	0.06	2.33	4.82	15.84	2.66	18.22	0.04	3.69	4.35	11.65	2.38	13.31
	S	AV	0.33	277.73	41.41	93.23	0.51	142.58	0.36	270.54	43.03	100.49	1.12	125.90
		STD	0.06	4.89	3.30	16.99	2.70	19.14	0.06	6.04	3.33	15.94	2.26	20.50
	E	AV	0.40	276.08	37.84	112.04	-8.75	134.96	0.50	268.96	41.76	139.61	-3.79	91.38
		STD	0.07	0.64	4.89	19.76	3.35	21.72	0.08	0.26	3.59	21.96	1.35	21.50
	RS	AV	0.39	286.50	44.43	108.97	-3.14	136.23	0.37	282.9	45.0	103.9	-2.5	136.6
		SD	0.08	7.65	7.28	21.48	4.16	23.43	0.07	10.7	6.3	19.9	4.0	26.0

			2019						2020					
SEASON	REGION		E(	QS	QB	QE	QC	QN	E	QS	QB	QE	QC	QN
			(CM/D)	W/m^2					(CM/D)	W/m^2				
AUT	N	AV	0.55	198.62	73.60	154.73	6.48	-36.20	0.62	198.92	75.52	172.50	7.65	-56.75
		STD	0.10	5.72	9.29	28.55	3.39	41.00	0.10	5.76	9.91	27.93	5.10	40.46
	C	AV	0.43	217.98	62.51	118.68	7.96	28.83	0.48	219.34	66.02	134.40	7.66	11.26
		STD	0.05	5.59	3.49	13.94	1.91	20.72	0.09	6.39	2.79	25.04	1.86	32.61
	S	AV	0.45	232.79	57.56	126.79	4.75	43.70	0.47	236.62	64.03	130.26	5.34	37.01
		STD	0.11	3.86	4.80	32.18	5.07	30.64	0.09	4.15	5.13	25.05	3.44	21.59
	E	AV	0.43	235.88	59.16	118.90	9.48	48.33	0.43	247.45	64.76	121.24	6.82	54.62
		STD	0.04	2.82	3.11	10.94	1.86	9.01	0.04	1.30	3.32	11.49	1.22	12.26
	RS	AV	0.46	219.02	63.46	129.65	6.79	19.12	0.51	221.6	67.6	141.3	6.9	5.8
		SD	0.10	14.22	8.30	27.96	3.75	43.00	0.11	16.5	7.4	30.6	3.5	48.6

Table 3. Average of evaporation and heat budget terms at different regions of the Red Sea during the years 2019- 2020

			2019						2020					
SEASON	REGION		E	QS	QB	QE	QC	QN	E	QS	QB	QE	QC	QN
			(CM/D)	W/m^2					(CM/D)	W/m^2				
YEAR	N	AV	0.57	243.22	73.97	158.85	7.62	2.79	0.51	244.53	72.57	143.12	5.70	23.15
		STD	0.08	2.65	8.82	21.77	4.06	31.34	0.07	2.99	8.18	19.02	3.78	28.16
	C	AV	0.46	252.17	59.83	128.47	5.71	58.17	0.45	252.51	60.93	125.10	5.37	61.11
		STD	0.08	2.90	4.75	21.33	3.07	30.23	0.06	1.98	3.87	15.70	2.12	21.26
	S	AV	0.36	257.20	52.48	100.86	2.32	101.53	0.38	254.78	54.96	106.75	3.70	89.37
		STD	0.08	0.91	2.91	21.89	2.91	19.91	0.06	0.85	3.33	16.62	2.17	15.52
	E	AV	0.37	259.77	51.74	102.07	1.95	104.01	0.41	256.97	53.47	113.77	3.05	86.69
		STD	0.04	1.20	3.39	10.87	1.68	12.57	0.04	1.15	2.80	11.68	0.84	12.31
	RS	AV	0.45	252.07	60.45	125.69	4.90	61.04	0.44	251.6	61.4	123.2	4.8	62.2
		SD	0.11	6.02	9.93	30.40	3.85	46.36	0.08	4.6	8.5	21.3	2.7	32.7

During spring

The evaporation rate starts to decrease in all regions compared to that recorded during winter, but with the same pattern, where it decreases southward. The average evaporation value over the Red Sea as a whole is nearly the same during the two years (0.32- 0.33cm/ day).

During summer

During this season, the evaporation rate starts to increase more than that during spring. It is higher at NRS-region and CRS-region during 2019 than that during 2020 (as winter, but with less value) and the reverse occurred in SRS-region and ERS-region. Additionally, it is noticed that the evaporation value decreases within the Red Sea southward and increases in the ERS-region. The value of the evaporation rate over the Red Sea as a whole is 0.39cm/ day during 2019, and 0.37cm/ day during 2020.

During autumn

During this season, the evaporation continues to increase than in the summer. The value of evaporation during 2020 is higher at NRS-region and lower at ERS-region. The average evaporation values over the Red Sea as a whole during this season are 0.46cm/ day during 2019, and 0.51cm/ day during 2020.

The average evaporation for the Red Sea (NRS-CRS-SRS) is 0.46± 0.19cm/ day (1.68m/ year) for 2019 and 0.443± 0.18cm/ day (1.62m/ year) for 2020. These results give average evaporation for the two years of about 1.65m/ year over the Red Sea. The corresponding values for the whole study area (4 regions) are 0.45± 0.19cm/ day (1.64m/ year) for 2019, and 0.44± 0.17cm/ day (1.61m/ year) for 2020, with an average value of about 1.63m/ year. These values of evaporation for the Red Sea are compatible with the previous studies of **Privett (1959)**, **Meshal *et al*. (1984)**, **Da Silva *et al*. (1994)**, **Tragou *et al*. (1999)**, **Al-Subhi (2012)**, **Ahmed and Albarakati (2015)** and **Nagy *et al*. (2021)**.

1.2 Seasonal heat budget terms

Tables (1- 3) show the seasonal average of heat budget terms at different regions of the study area and the Red Sea as a whole during 2019 and 2020. Note that, the heat gain by solar flux (Qs) with positive values in tables. The heat loss from the sea by long-wave terrestrial radiation (Qb), and latent heat flux (Qe) are written as positive value in the tables, nonetheless it means heat loss. The sensible heat flux (Qc) may be gained or lost depending on the sea-air temperature differences. When the sea water temperature is higher than air temperature (Tw > Ta), it results in heat loss and is listed in the tables as positive values and vice versa. Conversely, if Tw< , it indicates heat gain and is listed as negative values in the tables.

During winter

The solar flux (Qs) increases generally from north to south. The average value over the Red Sea as a whole is 214.8W/ m^2.

The long-wave radiation flux (back radiation) (Qb) decreases southward. The average value over the Red Sea as a whole is 76.5W/ m^2.

The latent heat flux (Qe) decreases southward. The maximum heat loss due to evaporation (224.5W/ m^2) is found at NRS-region during 2019, and the minimum average value (95.9W/ m^2) is observed at ERS-region. The average value of latent heat flux over the Red Sea as a whole during winter (average 2019 and 2020) is 153.8W/ m^2.

The sensible heat flux (Qc) showed a heat loss from the sea at all regions of the study area due to the higher water temperature than the air temperature. The maximum heat loss (24.7W/ m^2) is found at NRS-region during 2019. The value of Qc decreases from north to south within the Red Sea and increases at ERS-region. The average heat loss due to conduction during 2019 and 2020 over the Red Sea as a whole is 13.3W/ m^2.

The net heat flux (Qn) during winter showed a heat loss from the sea at NRS-region and CRS-region and a heat gain at SRS-region and ERS-region. The value of Qn increases southward. The maximum heat loss (157.6W/ m^2) is found at NRS-region during 2019. The maximum heat gain (76.4W/ m^2) is found at ERS-region during 2019. The average net heat flux (Qn) over the Red Sea as a whole is -34.8W/ m^2 during 2019 and -23.1W/ m^2 during 2020, with an average value of about -28.8W/ m^2.

Thus, during winter, over the Red Sea as a whole, the heat budget terms are as follows:

$Qs - Qb - Qe \pm Qc = 214.8\text{-}76.5\text{-}153.8\text{-}13.3 = -28.8$W/ m^2.

During spring

The short-wave solar radiation flux (Qs) is the highest at CRS-region and decreases slightly northward and southward to reach the lowest value at ERS-region. The average value of Qs over the Red Sea as a whole is 291.8W/ m^2.

The long-wave radiation flux (Qb) during spring is lower than during winter, and its value decreases also southward. The average value of Qb over the Red Sea as a whole is about 57.5W/ m^2.

The latent heat flux (Qe) decreases southward. The higher values (> 100W/ m^2) occurred at NRS-region during 2019 and 2020, while the lower one (about 77.5W/ m2) is found at ERS-region. The average value of Qe over the Red Sea as a whole is 90.8W/ m^2.

The sensible heat flux (Qc) during spring showed a heat gain at NRS-region and heat loss in the rest regions. The average value of the two studied years (2019– 2020) over the Red Sea as a whole gives a heat loss from the sea of about 1.2W/ m^2.

The net heat flux (Qn) showed a heat gain in all regions. For the Red Sea as a whole, the average net heat gain is 142W/ m^2.

Thus, the average heat budget terms over the Red Sea as a whole during spring are as follows:

$Qs - Qb - Qe \pm Qc = 291.8\text{-}57.5\text{-}90.8\text{-}1.2 = 142.3$W/ m^2.

During summer

During this season, the short wave solar radiation flux (Qs) decreases from north to south with an average value over the Red Sea as a whole of 284.7W/ m^2.

The long-wave radiation flux (Qb) decreases also southward, with the average value of 44.7W/ m^2 over the Res Sea as a whole.

The latent heat flux (Qe) is higher during 2019 (122.8W/ m^2) at NRS-region and during 2020 (139.6W/ m^2) at ERS-region. The lowest value of Qe during summer (93.2W/ m^2) is found at SRS-region. The average value of Qe over the Red Sea as a whole is 106.4W/ m^2.

The sensible heat flux (Qc) showed heat gain at all regions except at SRS-region where heat loss is observed. The average sensible heat flux (Qc) over the Red Sea as a whole gives a heat gain with a value of -2.8W/ m^2.

The net heat flux (Qn) is gained at all regions. The value of Qn during 2020 is higher than that during 2019 at NRS-region and CRS-region, and the reverse at the SRS-region and ERS-region where Qn during 2019 is higher. The average value of Qn over the Red Sea as a whole is 136.4W/ m^2.

Thus, the average heat budget terms over the Red Sea as a whole during summer are as follows:

$Qs - Qb - Qe \pm Qc = 284.7\text{-}44.7\text{-}106.4+2.8 = 136.4 W/ m^2$.

During autumn

The solar flux (Qs) increases southward. The maximum values are found at ERS-regions, with values of 235.9W/ m^2 during 2019 and 247.5W/ m^2 in 2020. The average value of Qs over the Red Sea as a whole is 220.3W/ m^2.

The long-wave radiation flux (Qb) decreases southward at the Red Sea regions and slightly increases at ERS-region. The values of Qb during 2020 are higher than those recorded during 2019. The average Qb over the Red Sea as a whole is 65.5W/ m^2.

The latent heat flux (Qe) decreases southward, and its value during 2020 is higher than that during 2019. The maximum heat loss due to evaporation (172.5W/ m^2) is observed at NRS-region during 2020. The minimum one (118.9W/ m^2) is found at ERS-region during 2019. The average Qe over the Res Sea as a whole is 135.5W/ m^2.

The sensible heat flux (Qc) is positive values at all regions. It means that there is heat loss from the sea by conduction due to higher sea water temperature than the air temperature. The average Qc over the Red Sea as a whole is 6.8W/ m^2.

Thus, the average heat budget terms over the Red Sea as a whole during autumn are as follows:

$Qs - Qb - Qe \pm Qc = 220.3\text{-}65.5\text{-}135.5\text{-}6.8 = 12.5 W/ m^2$.

During the year

The solar flux (Qs) during 2019 increases southward from 243.2W/ m2 at NRS-region to 259.8W/ m2 at ERS-region, with an average value (252W/ m^2) over the Red Sea as a whole. The value of Qs during 2020 is close to that during 2019, with an average value over the Red Sea of 251.6W/ m2. These values of Qs during 2019 and 2020 give an average Qs over the Red Sea as a whole of 251.8W/ m^2. This value is close to that calculated by **Bunker *et al.* (1982)**, **Tragou *et al.* (1999)**, **Matsukas *et al.* (2007)**, **Ahmed and Albarakati (2015)**, **AlSenafi *et al.* (2019)** and **Nagy *et al.* (2021)**.

The long-wave radiation flux (Qb) during the two studied years decreases southward from about 73W/ m^2 at NRS-region to about 52W/ m^2 at ERS-region. The average value of Qb during 2019 and 2020 over the Red Sea as a whole is 60.9W/ m^2. This value is close to that calculated by **Ahmed and Sultan (1989)**, **Ahmed *et al.* (1989)**, **Tragou *et al.* (1999)**, **Matsukas *et al.* (2007)** and **Ahmed and Albarakati (2015)**.

The latent heat flux (Qe) during the two years decreases also southward from > 140W/ m^2 at NRS-region to > 100W/ m^2 at ERS-region. The value of Qe during 2019 over the Red Sea as a whole is 125.7W/ m^2 and during 2020 is 123.2W/ m^2, with an average value of 124.4W/ m^2. This value is close to that calculated by **Bunker *et al.* (1982)**, **Tragou *et al.* (1999)**, **Matsukas *et al.* (2007)** and **Nagy *et al.* (2021)**.

The sensible heat flux (Qc) showed a heat loss from all regions during the two years, with higher values at NRS-region, and these values decrease southward. The average Qc value over the Red Sea as a whole is 4.85W/ m^2. This value coincides with that calculated by **Bunker (1976)**, **Bunker *et al.* (1982)**, **Ahmed *et al.* (1989)**, **Tragou *et al.* (1999)** and **AlSenafi *et al.* (2019)**.

The net heat flux (Qn) showed a heat gain in all regions. The average two years value of Qn over the Red Sea as a whole is 61.7W /m^2. This value coincides with that calculated by **Bunker (1976)**, **Bunker *et al.* (1982)**, **Tragou (1989)**, **Tragou *et al.* (1999)**, **Matsukas *et al.* (2007)**, **AlSenafi *et al* (2019)** (using ERA5 data through the period 2008-2010), and **Nagy *et al* (2021)** (at SRS-region).

Thus, the average heat budget terms over the Red Sea as a whole during the two years (2019-2020) are as follows:

$Qs - Qb - Qe \pm Qc = 251.8 - 60.9 - 124.4 - 4.9 = 61.6 W/m^2$.

2. Seasonal surface buoyancy flux

The net surface buoyancy flux (BF) includes contributions from both heat flux and freshwater flux at the sea surface. Positive buoyancy flux (BF> 0) indicates a buoyancy loss, it increases the density of surface layer and reduce stratification and drive convective mixing (i.e., water column is destabilized if BF> 0). While, the negative buoyancy flux (BF< 0) indicates a buoyancy gain, it decreases the density of surface layer and consequently increases the stability of water column and inhibits vertical mixing (i.e., water column stabilized if BF< 0).

The thermal, haline, and net surface buoyancy flux in the Red Sea are calculated monthly and seasonally. Furthermore, the absolute ratio between the thermal and haline components $|R|$ is calculated to recognize which of them is more effective on the net surface buoyancy flux.

i. The Red Sea region

The seasonal values of the net buoyancy flux and its thermal and haline flux components at different regions of the Red Sea during 2019- 2020 are presented in Table (4). From this table, it is observed that, the thermal and haline fluxes exhibit different seasonal variability and spatial patterns. The seasonal variability of the net buoyancy flux is mainly controlled by its thermal flux component, while the seasonal variability of haline flux component is much smaller. Higher evaporation during the winter reduces the near surface stratification and plays an important role in deepening the mixed layer.

The seasonal thermal buoyancy flux (BT) is positive during winter 2019 and 2020 at NRS and CRS regions and during autumn 2019 and 2020 at NRS-region. The maximum positive value ($11.37x10^{-8}$ m^2/ sec^3) is found at NRS-region during winter 2019. The negative thermal buoyancy flux is found during spring and summer at all regions, during winter at SRS and ERS-regions, and during autumn at CRS, SRS and ERS-regions. The maximum negative value ($-12.24x10^{-8}$ m^2/ sec^3) is observed at ERS-region during spring 2019 and 2020.

The thermal buoyancy flux over the Red Sea as a whole showed a positive value only during winter and negative ones during the rest of the seasons. The average values of the two years (2019- 2020) of thermal buoyancy flux (BT) are $2.70x10^{-8}$ m^2/ sec^3, $-11.0x10^{-8}$ m^2/ sec^3, $-11.33x10^{-8}$ m^2/ sec^3, and $-0.87x10^{-8}$ m^2/ sec^3 during winter, spring, summer, and autumn, respectively.

The seasonal haline buoyancy flux (BS) is positive over the Red Sea during all seasons. Its values decrease from north to south. The maximum value ($2.64x10^{-8}$ m^2/ sec^3) is found at NRS-region in winter 2019, while the minimum one ($0.84x10^{-8}$ m^2/ sec^3) is observed at ERS-region in spring 2019.

The seasonal haline buoyancy flux over the Red Sea as whole is generally small. The average seasonal values during winter, spring, summer, and autumn are $1.8\ x10^{-8}$ m^2/ sec^3, $1.0\ x10^{-8}$, $1.16\ x10^{-8}$, and $1.53\ x10^{-8}$ m^2/ sec^3, respectively.

The seasonal surface buoyancy flux is positive at NRS and CRS-regions during winter, at NRS-region during autumn, and at CRS-region during autumn 2020. It is negative at the rest of the regions and seasons. The maximum positive value ($14.01x10^{-8}$ m^2/ sec^3) is found during winter 2019 at NRS-region. The maximum negative value is $-11.40\ x10^{-8}$ m^2/ sec^3, and it is found at ERS-region during spring 2019- 2020.

The average seasonal values of surface buoyancy flux (BF) are $4.5x10^{-8}$ m^2/ sec^3 (winter), $-10.0x10^{-8}$ m^2/ sec^3 (spring), $-10.17x10^{-8}$ m^2/ sec^3 (summer), and $0.66x10^{-8}$ m^2/ sec^3 (autumn).

Table 4. Seasonal average of buoyancy components at different regions of the Red Sea during 2019- 2020

SEASON	YEAR	REGION		BT	BS	BF	SEASON	BT	BS	BF
				10^-8 m^2/sec^3				10^-8 m^2/sc^3		
WIN	2019	N	AV	11.37	2.64	14.01	SUM	-9.86	1.42	-8.44
			SD	3.26	0.39	3.63		2.47	0.28	2.75
		C	AV	4.12	1.95	6.07		-11.47	1.23	-10.24
			SD	5.37	0.59	5.96		1.45	0.17	1.61
		S	AV	-4.77	1.12	-3.65		-11.97	1.02	-10.95
			SD	1.71	0.28	1.98		1.58	0.19	1.76
		E	AV	-5.72	1.04	-4.68		-10.89	1.22	-9.68
			SD	0.92	0.1	1.01		1.7	0.22	1.9
		RS	AV	3.19	1.87	5.06		-11.21	1.21	-10
			SD	7.32	0.74	8.05		1.97	0.26	2.22
	2020	N	AV	7.68	2.16	9.84		-11.32	1.21	-10.12
			SD	2.55	0.3	2.83		2.31	0.28	2.59
		C	AV	3.08	1.83	4.91		-12.21	1.08	-11.13
			SD	3.15	0.35	3.49		1.07	0.12	1.18
		S	AV	-3.69	1.21	-2.48		-10.57	1.1	-9.47
			SD	1.36	0.2	1.53		1.68	0.18	1.85
		E	AV	-4.93	1.11	-3.83		-7.56	1.52	-6.03
			SD	0.75	0.09	0.83		1.78	0.24	2.02
		RS	AV	2.13	1.72	3.85		-11.47	1.12	-10.35
			SD	5.05	0.47	5.51		1.79	0.2	1.96
SEASON	YEAR	REGION		BT	BS	BF	SEASON	BT	BS	BF
SPR	2019	N	AV	-8.96	1.21	-7.74	AUT	2.76	1.78	4.55
			SD	1.81	0.21	2.02		3.16	0.33	3.48
		C	AV	-11.65	0.93	-10.71		-2.43	1.32	-1.11
			SD	1.42	0.14	1.55		1.7	0.16	1.85
		S	AV	-12.19	0.97	-11.23		-3.59	1.4	-2.19
			SD	1.89	0.27	2.16		2.46	0.35	2.79
		E	AV	-12.24	0.84	-11.4		-3.9	1.3	-2.6
			SD	0.68	0.07	0.75		0.73	0.12	0.83
		RS	AV	-11.12	1.02	-10.11		-1.46	1.46	0.01
			SD	2.12	0.24	2.34		3.48	0.34	3.79
	2020	N	AV	-9.22	1.15	-8.07		4.31	1.96	6.27
			SD	1.7	0.2	1.89		3.12	0.32	3.43
		C	AV	-10.86	1.02	-9.84		-1.03	1.5	0.47
			SD	1.42	0.14	1.55		2.67	0.28	2.95
		S	AV	-12.02	0.97	-11.05		-3.05	1.44	-1.61
			SD	1.55	0.2	1.75		1.71	0.27	1.96
		E	AV	-12.24	0.84	-11.4		-4.38	1.32	-3.06
			SD	1.24	0.13	1.37		0.97	0.13	1.09
		RS	AV	-10.8	1.04	-9.76		-0.29	1.6	1.31
			SD	1.86	0.19	2.03		3.81	0.36	4.15

Finally, the surface buoyancy flux over the study area can be summarized as follows:

Surface buoyancy loss in the Red Sea starts in early autumn, driven predominantly by surface cooling. Both thermal and haline fluxes exhibit a north–south gradient, with higher values in the NRS-region. The wintertime buoyancy loss is strong in the Gulf of Aqaba and in the northwestern part of the NRS-region, where the monthly mean heat fluxes during winter (January 2020) exceed -320W/ m^2, and evaporation can be as strong as 0.92cm/ day ($3.3my^{-1}$). They are driven by northwest cold air. The buoyancy loss increasing near the coasts in the CRS and NRS is mainly driven by the evaporation due to the dry winds blowing through mountain gaps. In contrast to the rest of the Red Sea, the sea surface in the SRS and ERS-regions gains buoyancy even during winter, when warmer southerly winds isolate it from the cooler atmospheric systems of the North **(Langodan *et al.*, 2017)**. In spring, most of the Red Sea gains buoyancy by heating from the atmosphere, especially in the SRS and ERS-regions. In summer, buoyancy gains at all regions of Red Sea due to higher air temperature than water temperature. In autumn, there is buoyancy loss at NRS and CRS-regions and a buoyancy gain at SRS and ERS regions.

ii. Annual buoyancy flux

The horizontal distributions of the Qn and buoyancy flux components over the Red Sea during 2019- 2020 are discussed in Table (5). Table (5) shows the annual buoyancy flux components over the Red Sea during 2019 and 2020. The thermal buoyancy flux showed a buoyancy gain over the Red Sea throughout the two years (2019- 2020). The maximum value of thermal buoyancy gain ($-8.4x10^{-8}$ m^2/ sec^3) is found at ERS-region during 2019. The average thermal buoyancy over the Red Sea as a whole is about $-4.87x10^{-8}$ m^2/ sec^3.

The haline buoyancy flux is positive throughout the two studied years. The maximum haline flux value is $1.85x10^{-8}$ m^2/ sec^3 which is observed at NRS-region during 2019. The average haline buoyancy over the Red Sea as a whole is $1.42x10^{-8}$ m^2/ sec^3.

The net (total) surface buoyancy flux (BF) over the Red Sea throughout the two years showed a buoyancy loss only at NRS-region during 2019, with value of $1.32x10^{-8}$ m^2/ sec^3 and a buoyancy gain at the rest regions, with a maximum value of $-7.3 x10^{-8}$ m^2/ sec^3 at ERS-region during 2019. The average net surface buoyancy flux over the Red Sea as a whole showed a heat gain with value of $-3.45x10^{-8}$ m^2/ sec^3. It means that, during the period of study (2019- 2020) the Red Sea as a whole is more buoyant i.e. its surface density decreases and its water column is stable and inhibits vertical mixing.

Finally from Tables (4, 5), it is clear that, the buoyancy forcing over the Red Sea is predominantly driven by its heat flux (thermal) component. Although haline fluxes (driven primarily by evaporation) in the RS region dominate the annually averaged surface buoyancy forcing, its seasonal variability is too weak to significantly affect the seasonal variability of the total buoyancy flux.

During winter, the buoyancy loss is strong in the NRS-region, where the net mean heat fluxes is negative (Qn< 0), and evaporation rates are high. During spring, warmer and lighter water is formed in the upper surface in response to the increasing solar radiation and a net heat flux entering the ocean (Qn> 0). This positive heat flux creates a buoyant and shallow mixed layer that traps the warm surface waters, increasing the stratification of the upper ocean and continuing to intensify throughout spring. During summer, the warmer and lighter water still predominated over the Red Sea, which makesthe surface layer of the Red Sea more buoyant, contributing to stable conditions. During autumn, the surface water starts to decrease due to decreasing solar radiation and increasing evaporation rate. This leads to cooling and denser surface water, especially at the northern part of the Red Sea and makes the water less buoyant, and the water column becomes unstable.

Table 5. The average values of buoyancy components at different regions of the Red Sea during 2019-2020

SEASON	REGION		BT	BS	BF
			10^-8 m^2/sec^3		
YEAR	2019	N	-0.53	1.85	1.32
			2.31	0.25	2.55
		C	-4.8	1.44	-3.36
			2.36	0.25	2.61
		S	-8.17	1.11	-7.06
			1.6	0.23	1.83
		E	-8.4	1.1	-7.3
			0.8	0.12	0.92
		RS	-4.78	1.44	-3.34
			3.58	0.37	3.95
	2020	N	-2.03	1.64	-0.39
			2.09	0.22	2.3
		C	-5.03	1.39	-3.63
			1.67	0.18	1.85
		S	-7.23	1.17	-6.06
			1.25	0.18	1.42
		E	-7.05	1.23	-5.81
			0.95	0.13	1.08
		RS	-4.96	1.39	-3.58
			2.57	0.26	2.83

iii. The absolute buoyancy ratio (|R|)

The buoyancy flux (BF), determines the stability of the upper ocean, moreover it is possible to determine whether the thermal (BT) or haline (BS) component is the main contributor.

Seasonal values of the ratio $|R|$ at different regions of the Red Sea during 2019-2020 are shown in Table (6). It is shown that the buoyancy flux is mostly driven by the thermal term (BT). The thermal component is relatively higher than the haline component, and the net buoyancy follows a more or less similar pattern of thermal buoyancy all along the Red Sea.

Table (7) shows the average two years (2019- 2020) of seasonal evaporation, net heat flux, buoyancy flux components, the ratio $|R|$, and percent of thermal and haline components at different regions of the Red Sea.

Table 6. Seasonal values of the ratio $|R|$ at different regions of the Red Sea during 2019- 2020

YEAR	SEASON	REGION	$\|R\|$	BT-%	BS-%	YEAR	SEASON	REGION	$\|R\|$	BT-%	BS-%
2019	WIN	N	4.32	81.19	18.81	2020	WIN	N	3.55	78.02	21.98
		C	2.11	67.81	32.19			C	1.68	62.70	37.30
		S	4.27	81.02	18.98			S	3.05	75.31	24.69
		E	5.52	84.66	15.34			E	4.46	81.69	18.31
	SPR	N	7.39	88.08	11.92		SPR	N	8.02	88.91	11.09
		C	12.50	92.59	7.41			C	10.61	91.39	8.61
		S	12.61	92.65	7.35			S	12.38	92.53	7.47
		E	14.54	93.56	6.44			E	14.56	93.57	6.43
	SUM	N	6.96	87.43	12.57		SUM	N	9.39	90.38	9.62
		C	9.35	90.34	9.66			C	11.27	91.85	8.15
		S	11.75	92.16	7.84			S	9.61	90.58	9.42
		E	8.96	89.96	10.04			E	4.96	83.22	16.78
	AUT	N	1.55	60.77	39.23		AUT	N	2.20	68.72	31.28
		C	1.84	64.79	35.21			C	0.69	40.67	59.33
		S	2.57	71.96	28.04			S	2.12	67.94	32.06
		E	3.00	75.03	24.97			E	3.32	76.86	23.14
	YEAR	N	0.28	22.13	77.87		YEAR	N	1.24	55.35	44.65
		C	3.34	76.96	23.04			C	3.61	78.32	21.68
		S	7.37	88.05	11.95			S	6.16	86.03	13.97
		E	7.65	88.44	11.56			E	5.71	85.11	14.89

\

Table 7. Average two years (2019- 2020) of seasonal buoyancy flux parameters at different regions of the Red Sea

SEA	REG	AVERAGE 19-20							
SON		E	QN	BT	BS	BF	|R|	BT-%	BS-%
		cm/d	W/m^2	10^-8 m^2/ sec^3					
WIN	N	0.74	-133.15	9.53	2.40	11.93	3.97	79.87	20.13
	C	0.60	-47.86	3.60	1.89	5.49	1.90	65.57	34.43
	S	0.38	56.31	-4.23	1.17	-3.07	3.63	78.41	21.59
	E	0.35	71.04	-5.33	1.08	-4.26	4.95	83.20	16.80
	RS	0.56	-37.10	2.66	1.80	4.46	1.48	59.71	40.29
SPR	N	0.37	124.59	-9.09	1.18	-7.91	7.70	88.51	11.49
	C	0.32	144.54	-11.26	0.98	-10.28	11.54	92.03	7.97
	S	0.32	151.27	-12.11	0.97	-11.14	12.48	92.58	7.42
	E	0.28	152.22	-12.24	0.84	-11.40	14.57	93.58	6.42
	RS	0.33	141.51	-10.96	1.03	-9.94	10.64	91.41	8.59
SUM	N	0.41	132.99	-10.59	1.32	-9.28	8.05	88.95	11.05
	C	0.38	144.48	-11.84	1.16	-10.69	10.25	91.11	8.89
	S	0.35	134.24	-11.27	1.06	-10.21	10.63	91.40	8.60
	E	0.45	113.17	-9.23	1.37	-7.86	6.73	87.07	12.93
	RS	0.38	138.30	-11.34	1.17	-10.18	9.73	90.68	9.32
AUT	N	0.59	-46.48	3.54	1.87	5.41	1.89	65.40	34.60
	C	0.46	20.05	-1.73	1.41	-0.32	1.23	55.10	44.90
	S	0.46	40.36	-3.32	1.42	-1.90	2.34	70.04	29.96
	E	0.43	51.48	-4.14	1.31	-2.83	3.16	75.96	24.04
	RS	0.49	9.28	-0.88	1.53	0.66	0.57	36.38	63.62
YEAR	N	0.54	12.97	-1.28	1.75	0.47	0.73	42.31	57.69
	C	0.46	59.64	-4.92	1.42	-3.50	3.47	77.65	22.35
	S	0.37	95.01	-7.70	1.14	-6.56	6.75	87.10	12.90
	E	0.39	97.23	-7.73	1.17	-6.56	6.63	86.90	13.10
	RS	0.45	58.95	-4.87	1.42	-3.46	3.44	77.49	22.51

CONCLUSION

The monthly and seasonal heat and buoyancy fluxes at the different regions and over the Red Sea as a whole are calculated using ERA5 meteorological data and HYCOM surface water temperature and salinity data during two years, 2019 and 2020. The result revealed that:

The evaporation rate in the Red Sea gradually decreases from north to south. The northern and central Red Sea has higher evaporations during the winter (0.80cm/ day and 0.62cm/ day, respectively) and moderate evaporations (~0.42cm/ day) during the summer. Evaporation shows weak seasonality in the southern Red Sea (~0.34cm/ day). The annual average evaporation rate for the Red Sea as a whole is 0.45cm/ day (1.64 m/ year).

The short-wave solar flux (Qs) increases from north to south. The monthly net solar flux Qs has significant seasonality, taking its smallest value (~157Wm^{-2}) in winter, and its largest (~310Wm^{-2}) in summer. The annual mean of short-wave solar radiation for the Red Sea as a whole is ~252Wm^{-2}.

The summer-winter variation of long-wave radiation (Qb) is small and it gradually decreases from north to south. The largest Qb fluxes are seen in the NRS- region (~0.97W/ m^2 during winter) and the lowest value is found at ERS-region (~38W/ m^2 during summer). The net terrestrial flux Qb does not exhibit large seasonal variations, having a value of about 61Wm^{-2} throughout the year.

The latent heat flux (Qe) during the two years decreases also southward from ~140W/ m^2 at NRS-region to ~100W/ m^2 at ERS-region. The average value of Qe is about 124.4W/ m^2.

The sensible heat flux (Qc) showed a heat gain during summer months and heat loss during the rest months. The largest heat gain during the winter (22Wm^{-2}) is found at NRS-region and the largest heat loss (-8.75W/ m^2) during the summer is observed at ERS-region. The magnitude of sensible heat flux is generally small. The average Qc value over the Red Sea as a whole is 4.85W/ m^2.

In winter, the net heat flux is negative, which means that the sea surface loses heat into the atmosphere. Starting from March-April to October, the net heat flux changes its sign, and the sea surface begins to gain heat from the atmosphere. The annual mean of net heat flux (Qn) for the Red Sea as a whole showed a heat gain, with an average value of about 61.6Wm^{-2}.

The surface buoyancy flux (BF) is mostly driven by the thermal term (BT). The thermal component is relatively higher than the haline component, and the net buoyancy follows a more or less similar pattern of thermal buoyancy all along the Red Sea.

The thermal and haline fluxes exhibit different seasonal variability and spatial patterns. The seasonal variability of the net buoyancy flux is mainly controlled by its thermal flux component, while the seasonal variability of haline flux component is much

smaller. Higher evaporation during the winter reduces the near surface stratification and plays an important role in deepening the mixed layer.

The net surface buoyancy flux also destabilizes the water column in January, February, November and December, which is an indication of the generation of strong convective mixing. It stabilizes the water column in the rest of the year, which is an indication of stratification of water column and shallow mixed layer depths.

REFERENCES

Ahmad, F., and Albarakati, A. M. A. (2015). Heat Balance of the Red Sea. In N. M. A. Rasul and I. C. F. Stewart (Eds.), The Red Sea: The Formation, Morphology, Oceanography and Environment of a Young Ocean Basin (pp. 355–361). Berlin, Heidelberg: Springer Berlin Heidelberg. https://doi.org/10.1007/978-3-662-45201-1_21.

Ahmad F, and Sultan S.A.R (1989) Sea surface fluxes and their comparison with the oceanic heat flow in the Red Sea. Oceanol Acta 12(1):33–36.

Ahmad F.; S.A.R. Sultan and M.O. Moammar (1989). Monthly Variations of Net Heat Flux at the Air-Sea Interface in Coastal Waters Near Jeddah, Red Sea. Atmosphere-Ocean 27 (2): 406-413.

Al Senafi F.; Anis and V. Menezes (2019). Surface Heat Fluxes over the Northern Arabian Gulf and the Northern Red Sea: Evaluation of ECMWF-ERA5 and NASA-MERRA2 Reanalyzes. *Atmosphere* 2019, *10*(9): 504. https://doi.org/10.3390/ atmos10090504.

Al-Subhi, A.M. (2012). Estimation of Evaporation Rates in the Southern Red Sea Based on the AVHRR Sea Surface Temperature Data JKAU: Mar. Sci., Vol. 23, (1): 77-89

Anitha, G.; Ravichandran, M. and Sayanna, R. (2008) Surface Buoyancy Flux in Bay of Bengal and Arabian Sea. Annales Geophysicae, 26: 395-400. https://doi.org/10.5194/angeo-26-395-2008

Bleck, R (2002). An oceanic general circulation model framed in hybrid isopycnic-Cartesian Coordinates. Ocean Model. 2002, 4: 55–88.

Bunker AF (1976). Computation of surface energy flux and annual air-sea interaction cycles of the North Atlantic Ocean. Mon Weather Rev 104:1122–1140.

Bunker AF; Charnock H,and Goldsmith RA (1982) A note on the heat balance of the Mediterranean and Red Sea. J Ma Res Suppl 40:73–84.

Chassignet E.; Linda T, and Halliwell G.. (2003) North Atlantic Simulations with the Hybrid Coordinate Ocean Model (HYCOM): Impact of the Vertical Coordinate Choice, Reference Pressure, and Thermobaricity. J.phys.oceano., 33:2504-2526.

Cronin, M.F. and Sprintall, J. (2001) Wind and Buoyancy-Forced Upper Ocean. In: Steele, J.H., Ed., Elements of Physical Oceanography, Academic Press, Cambridge, pp.3217-3224.https://doi.org/10.1006/rwos.2001.0157

Cronin, M. F., and Sprintall, J. (2008). Wind- and Buoyancy-Forced Upper Ocean. Encyclopedia of Ocean Sciences, pp.337–345. https://doi.org/10.1016/B978-012374473-9.00624-X

da Silva AM; Young CC and Levitus S (1994) Atlas of surface marine data 1994, NOAA Atlas, NESDIS 6-10. U.S. Government Printing Office, Washington DC (5 volumes).

Emery, J.W.; L.D. Talley and G.L. Pickard, (2005). Descriptive physical oceanography (chapter-5), Water, Salt and Heat Budget of the Ocean Elsevier Descriptive physical oceanography, Elsevier.

Garcia H E; Boyer T P; Baranova O K; Locarnini R A; Mishonov A V; Grodsky A; Paver C R; Weathers K W; Smolyar I V' Reagan J R; Seidov D and Zweng M M. (2019). World Ocean Atlas 2018: Product Documentation. Mishonov A., Technical Editor

Geng, B.; Xiu, P., Shu; C.; Zhang W.Z.; Chai F.; Li, S. and Wang, D. (2019) Evaluating the Roles of Wind- and Buoyancy Flux-Induced Mixing on Phytoplankton Dynamics in the Northern and Central South China Sea. Journal of Geophysical Research: Oceans, 124: 680-702. phttps://doi.org/10.1029/2018JC014170

Gill, A.E. (1982) Atmosphere-Ocean Dynamics. International Geophysics Series, Academic Press, New York.

Halliwell G. (2004). Evaluation of vertical coordinate and vertical mixing algorithms in the Hybrid -Coordinate Ocean Model (HYCOM). Ocean Modeling, Vol.7, issues 3-4, pp.285-322. https://doi.Org/10.1016/j.ocemod.2003.10.002

Hersbach, H.; Bell, B.; Berrisford, P.; Hirahara, S.; Horányi, A.; Muñoz-Sabater, J.; Nicolas, J.; Peubey, C.; Radu, R. and Schepers, D.(2020). The ERA5 global reanalysis. Q. J. R. Meteorol. Soc. 2020, 146: 1999–2049.

Kara, A.B., (2004). Notes and Correspondence Stability-Dependent Exchange Coefficient for Air-Sea Fluxes, Journal of Atmospheric and Oceanic Technology, 22: 1080-1094.

Karstensen, J. and Lorbacher, K. (2011) A Practical Indicator for Surface Ocean Heat and Freshwater Buoyancy Fluxes and Its Application to the NCEP Reanalysis Data. Tellus A, 63: 338-347. https://doi.org/10.1111/j.1600-0870.2011.00510.x

MacIntyre, S.; Jonsson, A.; Jansson, M.; Aberg, J.; Turney, D.E. and Miller, S.D. (2010) Buoyancy Flux, Turbulence, and the Gas Transfer Coefficient in a Stratified Lake. Geophysical Research Letters, 37: L24604. https://doi.org/10.1029/2010GL044164

Matsoukas, C.; Banks, A.C.; Pavlakis, K.G.; Hatzianastassiou, N.; Stackhouse, Jr. P.W. and Vardavas, I. (2007) Seasonal Heat Budgets of the Red and Black Seas, Journal of Geophysical Research, 112: 1-15. C10017, doi:10.1029/200 6JC003849.

Mehrfar, H.; H. Morovvati, M. Torabi Azad, (2007). Study & Formulation of Heat Budget in Gorgan Bay in Fastest Wind Situation .J. of Sciences, Islamic Azad University, 17(63): 19-31.

Meshal A.H.; A.K.A. Behairy and M.M. Osman (1984). Evaporation From Coastal and Open Waters of the Central Zone of the Red Sea. ATMOSPHERE-OCEAN 22 (3) 1984, 369-378 0705-5900/84/0000-0369$01.25/0.

Nagy, H.; Mohamed, B.; Ibrahim, O. (2021). Variability of Heat and Water Fluxes in the Red Sea Using ERA5 Data (1981–2020). J. Mar. Sci. Eng. 9: 1276. https://doi.org/

Naoki Hirose; C. Kim, and J.H. Yoon, (1996). Heat Budget in the Japan Sea, Journal of ceanography, 52: 553-574.

Privett DW (1959) Monthly charts of evaporation from the North Indian Ocean, including the Red Sea and Persian Gulf. Q J Roy Meteorol Soc 85:424–428.

Simonsen K. and M., Haugan, (1996). Heat Budgets of the Arctic Mediterranean and sea surface heat flux parameterizations for the Nordic Seas, Journal of Geophysical Research, 101(C3): 6533-6576.

Tragou E.; C. Garrett, and R. Outerbridge (1999). The Heat and Freshwater Budgets of the Red Sea. Journal of Physical Oceanography, Vol 29 (10). 2504-2522.

Zhang, H.M. and Talley, L.D. (1998) Heat and Buoyancy Budgets and Mixing Rates in the Upper Thermocline of the Indian and Global Oceans. Journal of Physical Oceanography, 28: 1961-1978. https://doi.org/10.1175/1520-0485(1998)028<1961: HABBAM>2.0.CO;2